ORIGINAL RESEARCH

Ultrasmall gold nanorods: synthesis and glycocalyx-related permeability in human endothelial cells

Ming J Cheng[1,*]
Nandita N Bal[1,*]
Priya Prabakaran[1]
Rajiv Kumar[2,3]
Thomas J Webster[1,4]
Srinivas Sridhar[1,2]
Eno E Ebong[1,2,5]

[1]Department of Chemical Engineering, Northeastern University, Boston, MA, USA; [2]Department of Physics, Northeastern University, Boston, MA, USA; [3]Millipore Sigma, Milwaukee, WI, USA; [4]Center of Excellence for Advanced Materials Research, King Abdulaziz University, Jeddah, Saudi Arabia; [5]Department of Neuroscience, Albert Einstein College of Medicine, New York, NY, USA

*These authors contributed equally to this work

Correspondence: Eno E Ebong
Department of Chemical Engineering, Northeastern University, 360 Huntington Avenue, 313 Snell Engineering Building, Boston, MA 02115, USA
Tel +1 617 373 8744
Fax +1 617 373 2209
Email e.ebong@northeastern.edu

Background: Clinical data show shed endothelial glycocalyx (GCX) components in blood samples of atherosclerotic patients, linking atherosclerotic development to endothelial GCX integrity. Healthy GCX has pores no >7 nm, and shed GCX has even larger pores. Therefore, we suggest targeting and treating atherosclerosis-prone blood vessels by using nanoscale vehicles to deliver drugs via the nanoscale GCX as it becomes dysfunctional.

Materials and methods: To test our idea, we investigated permeability of nanoparticles in endothelium, as related to a GCX expression. The present work involves nanorods, which are expected to interact with larger portions of endothelial cell (EC) membranes, due to surface area of the nanorod long axis. Conventional nanorod diameters are orders of magnitude larger than the GCX pore size, so we adapted conventional synthesis methods to fabricate ultrasmall gold nanorods (GNRs). Our ultrasmall GNRs have an aspect ratio of 3.4, with a length of 27.9±3.1 nm and a diameter of 8.2±1.4 nm. In addition, we produced GNRs that are biocompatible and fluorescently visible, by coating the surface with functionalized polyethylene glycol and Alexa Fluor 647. To study GNR–GCX interactions, we used human ECs, for species relevance.

Results: Under life-like flow conditions, the human ECs are densely covered with a 1.3 μm thick layer of GCX, which coincides with minimal GNR permeability. When the GCX is weakened from lack of flow (static culture) or the presence of GCX degradation enzyme in the flow stream, the GCX shows 40% and 60% decreased thickness, respectively. GCX weakness due to lack of flow only slightly increases cellular permeability to GNRs, while GCX weakness due to the presence of enzyme in the flow leads to substantial increase in GNR permeability.

Conclusion: These results clarify that the GCX structure is an avenue through which drug-carrying nanoparticles can be delivered for targeting affected blood vessels to treat atherosclerosis.

Keywords: human endothelial cells, gold nanoparticles, nanorods, glycocalyx, heparan sulfate

Introduction

Atherosclerosis is a disease characterized by blood vessel wall thickening and hardening due to growth of plaques filled with infiltrated lipids and other unwanted substances.[1] The disease affects millions of adults in the USA[2] and more worldwide. Precursors to atherosclerosis include dysfunction of the vasculoprotective endothelial cell (EC) lining of the inner blood vessel wall[3] and loss of the EC surface-attached glycocalyx (GCX)[3–6] that is involved in regulating vascular permeability.[7]

The endothelial GCX is a sugar-based nanoscale structure.[7] A healthy GCX has a pore size of 7 nm.[8,9] In diseased or dysfunctional conditions, the pore sizes increase, allowing for enhanced permeability through to the ECs and other parts of the blood
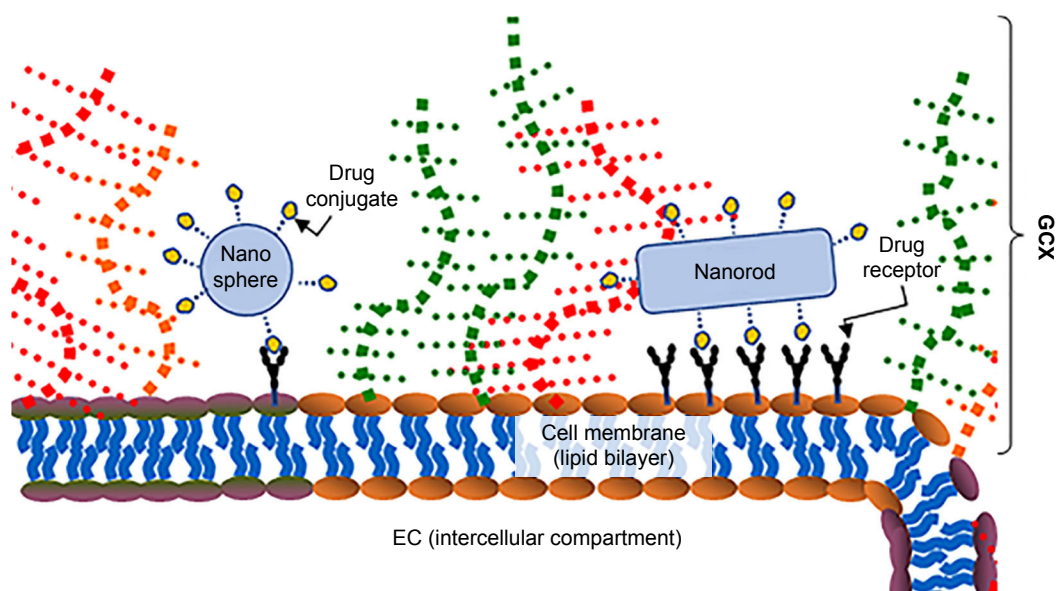
Figure 1 The motivation of this study: previously, we studied GCX-dependent EC interactions with nanospheres, which could be used for targeted delivery of cardiovascular drug treatment to the ECs. The present work is a study of GCX-dependent EC interactions with nanorods, which when compared to nanospheres are expected to deliver cardiovascular drugs to a larger area of the ECs.
Abbreviations: EC, endothelial cell; GCX, glycocalyx.

vessel wall.[8,9] Just as GCX dysfunction coincides with atherosclerosis plaque initiation and growth, the increase in GCX permeability may present a potential avenue for enhanced delivery of anti-atherosclerotic treatments. Therefore, we suggest targeting and treating atherosclerosis-prone blood vessels by using nanoscale vehicles to deliver drugs via the nanoscale GCX pores as they grow due to conditions of dysfunction.

Nanotechnology has soared within the past two decades, with countless applications in a wide range of fields, from semiconductors[10–12] to food science[13] to medicine.[14] Nanoparticle development, in particular, has grown with respect to new approaches for characterization and formulations, with an increase in a variety of available nanoparticle types.[15–20] Furthermore, for medical applications and improved intravascular drug delivery, it is now possible to fine-tune and control the drug-carrying nanoparticle physical parameters, including shape, in accordance with local structures in the regions of interest.

Rod-shaped nanoparticles have the advantage of long axes that have large surface areas for enhanced interaction with the ECs on blood vessel walls (Figure 1).[21] At present, the cetyltrimethylammonium bromide (CTAB)-based GNR synthesis protocols[22–36] produce GNRs with diameters that are too big for GCX-mediated permeability across the vessel wall. One common approach to GNR synthesis is the CTAB-mediated seed growth method used by Nikoobakht's and other research groups.[22–36] This method utilizes CTAB solution and chloroauric acid (HAuCl$_4$). Combining these chemicals creates an Au(III)–CTAB complex, due to formation of

an ion pair between the negatively charged AuCl$_4$ and the positive head groups of the CTAB micelles. The complex is reduced by ascorbic acid (HAuO$_2$),[37] resulting in the formation of rod-shape directing CTAB aggregates that act as a cage in which the nanoparticle seeds grow. In the present work, we aimed to develop gold nanorods (GNRs) that are ultrasmall, scaled in size for compatibility with the porosity of the GCX, while offering relatively a large surface area. We hypothesize that making these nanorods of a smaller size would enable them to better penetrate GCX nanospaces. To test our hypothesis, we observed and characterized the nature of our GNR interactions with ECs. We found that ultrasmall GNRs selectively penetrate human ECs that express severely dysfunctional GCX. Our finding suggests that a smaller nanoparticle size, combined with a rod shape and a high surface area, would increase GNR potential as drug delivery vehicles for intravascular applications.

Materials and methods
Selected materials

Chloroauric acid (HAuCl$_4$), L-ascorbic acid (C$_6$H$_8$O$_6$), silver nitrate (AgNO$_3$), CTAB, sodium borohydride (NaBH$_4$), sodium carbonate (Na$_2$CO$_3$), sodium bicarbonate (NaHCO$_3$), glutaraldehyde, and goat serum were all obtained commercially from Sigma. Heterofunctional thiol polyethylene glycol (PEG) terminating in amine and methoxy groups (PEG-NH$_2$ and PEG-CH$_3$) was purchased from Lysan Bio. Dialysis tubes with molecular weight cutoff of 12–14 kDa

were supplied by EMD Millipore, and Alexa Fluor 647 (AF-647) N-Hydroxysuccinimide (NHS) ester was provided by Molecular Probes. The 3-(4,5-dimethylthiazol-2-yl)-5-(3-carboxymethoxyphenyl)–2-(4-sulfophenyl)-2H-tetrazolium (MTS) assay was purchased from Promega. Cell culture materials including human umbilical vein endothelial cells (HUVECs), EC growth media (EGM-2), and EGM-2 supplements were purchased from Lonza. Heparinase III (Hep III) enzyme was purchased from IBEX Pharmaceutical, while paraformaldehyde for fixation was purchased from ACROS Organics. 10E4 epitope heparan sulfate (HS) mouse monoclonal IgM antibody was purchased from Ambsbio and the Alexa Fluor 488 (AF-488) goat anti-mouse IgG, IgM fraction, a secondary antibody, was purchased from Thermo Fisher Scientific. Vectashield mounting medium containing DAPI was purchased from Vector Laboratories. All experiments used ultrapure water with resistivity of 18.2 MΩ cm and containing no particulates >0.22 μm, which was obtained from a Milli-Q water purification system.

GNR synthesis

Three 50 mL conical tubes, each containing 765.3 mg of CTAB and 21 mL of water, were left in a 37°C water bath overnight to make a stock solution of 0.1 M CTAB, which forms the cage of the GNRs to be synthesized (Figure 2A). The next day, GNR seed and growth solutions were prepared from the 0.1 M CTAB. For the seed solution, after adding 10 μL of 25 mM $HAuCl_4$ to 990 μL of warm 0.1 M CTAB in a 2 mL microcentrifuge tube, the seed $HAuCl_4$–CTAB mixture was vortexed briefly (Figure 3). Six hundred microliters of ice-cold $NaBH_4$ were added to the seed $HAuCl_4$–CTAB mixture and vortexed again (Figure 3). The resulting light brown solution (Figure 3) was kept at room temperature. For the growth solution, after the addition 200 μL of 25 mM

$HAuCl_4$ to 10 mL of 0.1 M CTAB (Figure 3) in each of six 15 mL centrifuge tubes, the growth $HAuCl_4$–CTAB mixture was vortexed until the color of the solution turned clear orange (Figure 3). Addition of 300 μL of 4 mM $AgNO_3$ followed by 150 μL of 80 mM ascorbic acid to the growth $HAuCl_4$–CTAB mixture turned the solution colorless (Figure 3) after gentle mixing. Once both the seed and growth solutions were prepared, 12 μL of the seed solution was added to each tube of growth solution (Figure 3) and kept at 33°C. Within 15 minutes, the color of the solution mixture changed from clear to dark brown, indicating nanorod formation (Figure 3).[35] The solution mixture was left in the water bath for an additional hour, to finalize the formation of the rods. Afterwards, the six vials of mixed seed and growth solutions were centrifuged in the 15 mL centrifuge tubes, at 8,000 revolutions per minute (rpm) for 20 minutes. Once centrifugation was complete, the supernatant was carefully removed leaving behind pellets of nanorods. The pellets were resuspended in 1 mL of water, and centrifuged again at 7,000 rpm for 15 minutes, following Jessl et al's protocol.[27] This time, the pellets containing larger material, including large impurities and nanorods, were discarded. The supernatant was retained as it contained the desired ultrasmall GNRs.

The GNR was further modified by the addition of a PEG coat (Figure 2B), which enables downstream customization in future iterations of the GNRs. One milliliter of water was used to dissolve 7.5 mg of 3.4 kDa SH-PEG-NH$_2$ and 15 mg of 2 kDa SH-PEG-m in 6 mL of GNR solution. The PEG-GNR solution was stirred overnight, and then dialyzed against water for 2 days using 12–14 kDa molecular weight cutoff dialysis tubes, to remove unreacted PEG, CTAB, and other chemical reactants.

The amine functional group on the PEG coating was leveraged to conjugate a fluorophore onto the GNR (Figure 2C),
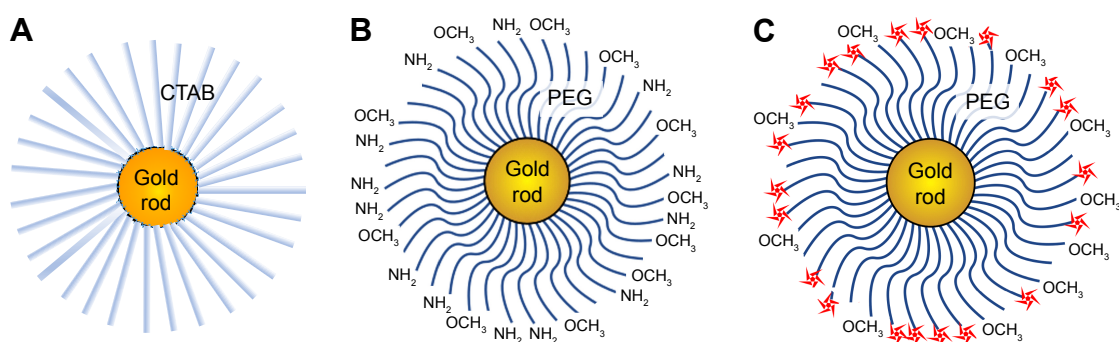

Figure 2 Schematics of synthesized GNRs.
Notes: (**A**) CTAB-coated GNRs, before PEG replacement. (**B**) PEGylated GNRs with two types of PEG terminations, including $-NH_2$ and $-OCH_3$. (**C**) AF-647 conjugated nanoparticles for fluorescence imaging. Red stars show the AF-647 conjugated to NH_2 functional groups.
Abbreviations: CTAB, cetyltrimethylammonium bromide; GNRs, gold nanorods; PEG, polyethylene glycol.

Chemical	Purpose	Stock concentration	Seed recipe[a]	Growth recipe[b]
CTAB	Surfactant that prevents nanoparticle clumping	0.100 M	0.990 mL	10 mL
$HAuCl_4$	Metallic solution, which contains GNR seed	0.025 M	0.010 mL	0.200 mL
$NaBH_4$	Toxic component that aids in reaction	0.010 M	0.600 mL	–
$C_6H_8O_6$	Regulates pH	0.080 M	–	0.150 mL
$AgNO_3$	Alters aspect ratio of GNR	0.004 M	–	0.300 mL

[a]Mixed in a 2-mL microcentrifuge tubes from which six 12-mL aliquots were obtained. One aliquot was added to one tube of growth solution.

[b]Mixed in each of six 15-mL centrifuge tubes. Each tube was supplemented with one aliquot of seed solution.
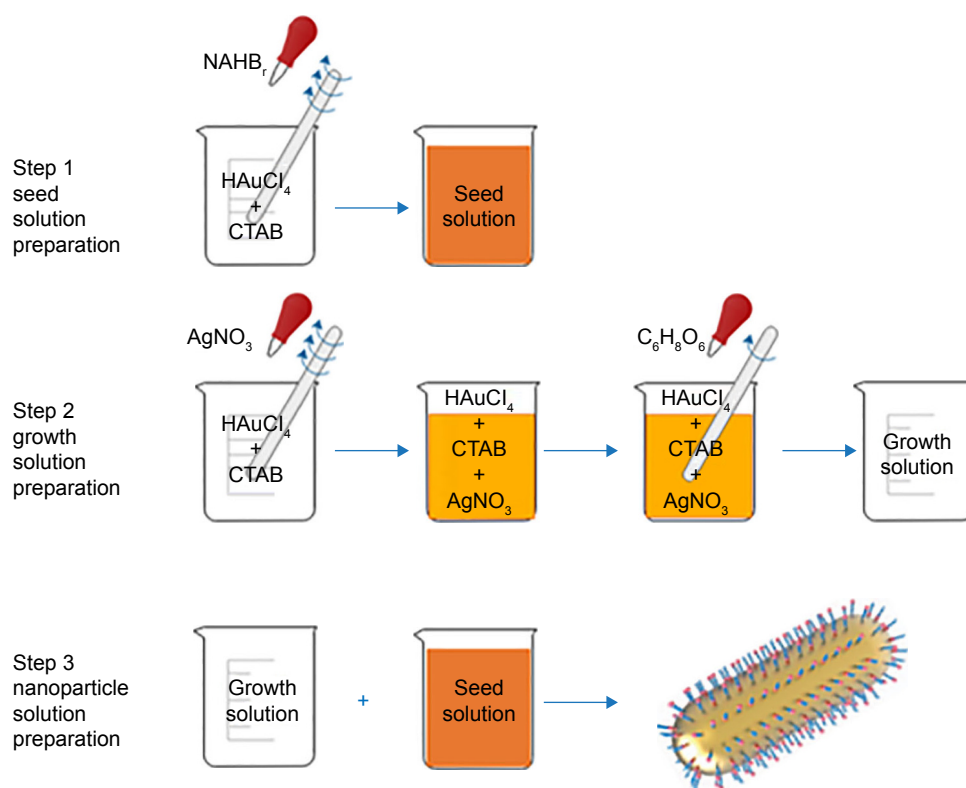

Figure 3 Our modified GNR synthesis protocol, which is intended to produce ultrasmall GNRs, is summarized here.
Notes: The table shows the core ingredients along with stock solution concentrations and the amounts to add to the GNR seed solution and the GNR growth solution. A flow diagram further clarifies the protocol for the synthesis of GNRs. The CTAB-coated GNR art was reprinted by permission from Springer Nature: *Light: Science & Applications*. He J, Zheng W, Ligmajer F, et al. Plasmonic enhancement and polarization dependence of nonlinear upconversion emissions from single gold nanorod@SiO2@CaF2:Yb3+,Er3+ hybrid core–shell–satellite nanostructures. Copyright 2017.[63]
Abbreviations: CTAB, cetyltrimethylammonium bromide; GNR, gold nanorod.

making visualization with fluorescence microscopy possible. To accomplish this, the dialyzed PEG-GNR solution was mixed with 300 µL of 0.1 M sodium carbonate and 0.8 µL of 10 mg/mL AF-647 conjugated NHS ester dissolved in dimethyl sulfoxide. The mixture was covered with foil and allowed to stir at room temperature overnight. The resulting solution was dialyzed for 2 days to remove excess fluorophore, lyophilized, and kept in a −20°C freezer until use.

For cell culture experiments, the GNRs were reconstituted and were passed through a 0.22 µm syringe filter for sterility.

GNR size and fluorescence characterization

The size and fluorescence of the PEGylated GNRs were characterized using 1 mg/mL of dried fluorescent GNRs dissolved in water. GNR sizes were assessed pre- and post-centrifugation,

using transmission electron microscopy (TEM). Fifteen microliters of 1 mg/mL GNR solution were dropped onto a carbon-coated, copper TEM grid and allowed to sit for 5 minutes before excess liquid was wicked off using filter paper. The TEM grids were subsequently loaded into a JEOL JEM-1000 microscope for TEM imaging at 80 kV and 120,000× magnification to observe and record GNR, for later quantification of GNR size. A NanoDrop Microvolume Spectrophotometer was used for aspect ratio measurements, using three separate batches of GNR. Using of 2 μL samples, absorbances from 220 to 750 nm were plotted and averaged. To confirm PEG-GNR fluorescence activity, 1 mL of 1 mg/mL GNR solution was examined using a Jobin Yvon Fluoromax 4 fluorometer, to measure and plot the profile of GNR fluorescence emission wavelengths in response to excitations up to 650 nm.

Gold nanosphere synthesis

Gold nanospheres were also synthesized for comparison to GNRs in a subset of experiments. Gold nanosphere synthesis methods were previously published.[7]

Cell culture

For optimized cell growth, HUVEC cultures were fed supplemented EGM-2 according to the manufacturer's (Lonza) instructions, and grown in a humidified, 37°C, 5% CO_2 environment. For cell passaging, ~100,000 cells were seeded into each new T25 flask containing 6 mL of media.

MTS assays were conducted to show biocompatibility of the GNRs to HUVECs. Cells were seeded into 18 wells in a 96-well plates at a density of 5,000 cells/cm² and grown until confluency for each time point. Three hundred microliters of GNRs in EGM-2 were prepared in various concentrations (0, 100, 250, 500, 750, and 1,000 μg/mL) and 100 μL was added into each well for triplicate measurements. After continued incubation for 2, 4, 8, 16, and 24 hours at 37°C, the media were replaced with 100 μL of fresh, EGM-2 and 20 μL of MTS reagent and allowed to incubate for 2 more hours at 37°C. Ninety-six-well plates were then imaged at 492 nm absorbance using a SpectraMax M3 plate reader. The absorbance values, which correlated to cellular metabolic activity, were normalized to the value obtained for a confluent HUVEC culture exposed to 0 μg/mL of GNR and plotted.

MTS assays showing biocompatibility of gold nanospheres to cultured ECs were reported in a previous publication.[7]

For experiments, 1 mg/mL of sterile fibronectin was used to coat 22×40 mm glass and promote adhesion, and HUVEC was seeded at 15,000 cells/cm² density on the fibronectin-coated glass. Confluent HUVEC layers were achieved in 3 days.

Flow and GCX conditions

To assess flow-conditioned HUVEC permeability to GNRs, confluent monolayers were placed into parallel plate flow chambers and exposed to constant fluid shear stress of 12 dynes/cm² for 16 hours. The fluid used was supplemented EGM-2 with added 0.5% BSA, such that HUVEC GCX could be stabilized. To assess HUVEC permeability to GNRs when GCX is deficient, we added to the circulating media degradation enzyme 1.25×10^{-6} IU/mL Hep III. We also assessed HUVEC permeability to GNRs in the absence of flow (static conditions), which is expected to render GCX deficiency.

Naoparticle permeability assay

After confluent HUVECs were exposed to flow conditions, flow and HepIII conditions, or static conditions for 16 hours, they were cultured with 500 μg/mL of GNRs for another 4 hours in the absence of flow to observe the extent of GNR infiltration. We previously performed permeability assays for 16 hours, so a pilot study was also performed to confirm that a 4-hour permeability experiment would be sufficient. In the pilot study, confluent static-conditioned HUVECs were treated with 500 μg/mL of GNRs for 2, 4, 8, or 16 hours. This pilot study confirmed that GNR infiltration in HUVEC is statistically similar when the 2-, 4-, 8-, and 16-hour time points are compared (Tables 1 and 2). Therefore, 4-hour permeability assays are sufficient. Longer permeability experiments are not ideal and expected to suffer from loss of the flow effect. This pilot study also compared GNR permeability to gold nanosphere permeability.

Immunocytochemistry

After the 4-hour HUVEC treatment with GNRs, the media containing excess nanoparticles not taken up by the HUVEC was drained and the coverslips were washed quickly with

Table 1 Time-dependent EC uptake of GC GNRs

Time of EC exposure to GNRs (hours)	Normalized uptake (mean ± SEM)
2	0.66±0.28
4	0.73±0.16
8	0.82±0.18
16	1.00±0.31

Notes: Nanoparticle uptake studies usually require at least 16 hours of cell-nanoparticle co-incubation. In this study, flow-conditioned cells are expected to lose the flow effect by 16 hours, so shorter term cell-nanoparticle co-incubation is required. To confirm assess HUVEC uptake of GNRs after short-term incubation, HUVEC cultures were incubated with 500 μg/mL GNR for 2, 4, 8, and 16 hours. GNR uptake was quantified by measuring GNR-derived red fluorescence (the AF-647, which is conjugated to the GNRs) in the HUVEC cells. All results are normalized by 16-hour conditions. N=5.
Abbreviations: EC, endothelial cell; GNRs, gold nanorods; HUVEC, human umbilical vein endothelial cell; SEM, standard error of the mean.

Table 2 Statistical analysis results of data reported in Table 1, for relative HUVEC uptake of GNRs after 2, 4, 8, and 16 hours of HUVEC-GNR co-incubation

Comparative GNR uptake, due to time (hours)	Significance (yes/no)	Summary (ns)	P-value
2 vs 16	No	ns	0.1573
4 vs 16	No	ns	0.3223
8 vs 16	No	ns	0.6472
2 vs 8	No	ns	0.7238
4 vs 8	No	ns	0.9336
2 vs 4	No	ns	0.9669

Note: ANOVA and Tukey's post hoc test were performed, indicating ns in GNR uptake when various GNR exposure times were compared.
Abbreviations: GNR, gold nanorod; HUVEC, human umbilical vein endothelial cell; ns, no statistical significance.

warm 1% BSA in PBS. Cells were fixed for 30 minutes with a solution of 2% paraformaldehyde and 0.1% glutaraldehyde in PBS, at room temperature. This was followed by three 5-minute PBS washes to remove excess aldehydes. HS was stained using 1:100 10E4 epitope anti-HS and 1:1,000 AF-488 conjugated goat anti-mouse IgG, IgM secondary antibody. The cells were then covered with glass microscope slides using Vectashield mounting medium containing DAPI, to label HUVEC nuclei.

Microscopy

Similar to our previous study[7] the blue, green, and far red confocal microscope channels were used to visualize the DAPI for nuclei, AF-488 for HS, and AF-647 for the GNRs, respectively. Z-stacks of the sample at intervals of 0.2 μm were used to create a z-projection in ImageJ. The thickness and coverage of the HS component of the GCX were measured using cross-sectional views and *en face* images, respectively, using previously mentioned methods.[7] Briefly, the perpendicular distance from HUVEC nucleus to the edge of green fluorescence were measured at random points in the cross-sectional views, while area fraction of green above the background noise was measured in *en face* view for the coverage. Total red signal in the *en face* images was used to quantify the nanoparticle uptake for the field of view.

Statistics

GNR measurements from TEM, ultraviolet-visible range (UV-vis), fluorometer, and MTS were measured in triplicate and repeated for every batch for a total of four measurements to ensure consistency. For GNR uptake, three experiments were conducted per condition. In each experiment, there were two samples of HUVEC layers, for duplicates. Measurements were taken from five fields of view per HUVEC layer, where each field of view yielded three values for GCX thickness, one value for GCX coverage, and one value for nanoparticle uptake. Data are shown as mean ± standard error of the mean. Data were analyzed for statistical significance by using ANOVA with an alpha value of 0.05, followed by Tukey's multiple comparison test, using GraphPad Prism software. Further details are described in Figures 4–7 and Table 2 captions.

Results and discussion
The newly synthesized GNRs are smaller in size than conventional GNRs

In this study, to seed ultrasmall GNRs we maintained a CTAB (0.1 M) to auric acid ratio that is 10 times smaller than that in the protocols of other contributors like Nikoobakht,[30] Ahmed,[38] Beji,[24] Park,[31] and Sharma.[39] While the formation of CTAB capped GNRs is the necessary first step in the GNR fabrication protocol, CTAB-based GNR batches often contain nonuniformly sized particles, which is a major concern for researchers across the field.[40–42] As expected, our CTAB-GNR synthesis protocol initially produced wide variability in nanorod sizes (Figure 4A). In addition, we utilized double centrifugation steps to produce pure GNR batch. In our implementation of the second centrifugation step, the rpm were set to separate particles that do not pellet at 8,000 rpm from those that do pellet at 7,000 rpm.[27] After the second centrifugation step, we collected and retained the supernatant, which contained GNR batches of consistent size (Figure 4B). Future studies are required to better understand the mechanism of the CTAB cage and subsequent GNR formation, for improved control of GNR synthesis and to better achieve pre-specified dimensions on a consistent basis.

We report that GNRs synthesized using our method yielded GNRs measuring 27.9±3.1 nm by 8.2±1.4 nm (Figure 4B and D). This is much smaller than the size of conventional GNRs. In comparison with our GNRs, the larger GNRs synthesized with the original Nikoobakht protocol[30] were shown to be significantly longer and wider, at ~40.2±4.1 nm by 15.9±1.8 nm, as shown in Figure 4C and D. The dimension of the short axis of our GNRs will enable endothelial targeting at the onset of GCX damage that is associated with endothelial dysfunction, when the GCX pore sizes increase beyond 7 nm. The dimension of the long axis of our GNRs, on the other hand, will prevent the particles from being readily taken up at the initial onset of GCX dysfunction. The positive trade-off, however, is that the surface
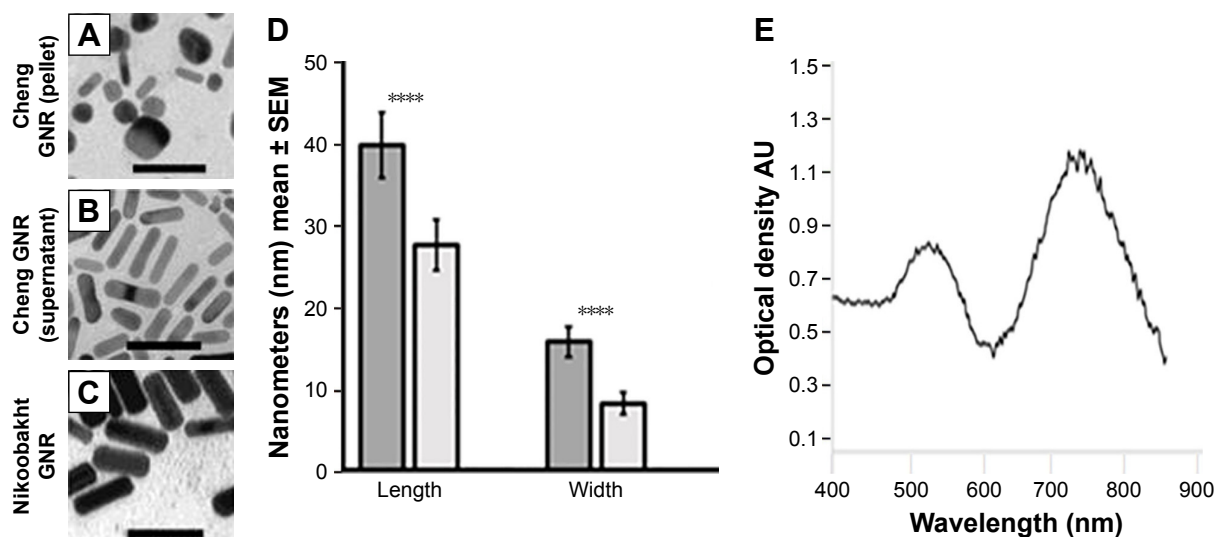
Figure 4 With our modified GNR synthesis protocol, we successfully achieved reduction in the length and width of GNRs, compared to previous protocols such as the one published by Nikoobakht et al.[30]
Notes: (**A**) TEM image of Nikoobakht's GNRs, scale bar 50 nm. (**B**) TEM image of impurities removed our GNR batch, found in the pellet after the secondary centrifuge at 7,000 rpm, scale bar 50 nm. (**C**) TEM image of our pure ultrasmall GNRs, found in the supernatant after the secondary centrifuge at 7,000 rpm, scale bar 50 nm. Reprinted with permission from Nikoobakht B, El-Sayed MA. Preparation and growth mechanism of gold nanorods (NRs) using seed-mediated growth method. *Chem Mater.* 2003;15(10):1957–1962. Copyright (2003) American Chemical Society.[30] (**D**) The quantification shows that Nikoobakht's GNRs were 40.2±4.1 nm long by 15.9±1.8 nm wide, while our ultrasmall GNRs measured 27.9±3.1 nm long by 8.2±1.4 nm wide. ****$P<0.0001$ between Nikoobakht's GNRs and our ultrasmall GNRs. N=3. (**E**) UV-vis of the ultrasmall GNRs. N=3, and the adsorption spectrum shown is a representative plot. The aspect ratio of 3.4 measured by TEM corresponds to what was calculated from the maximum absorption peak wavelength at about 740 nm.
Abbreviations: GNRs, gold nanorods; rpm, revolutions per minute; TEM, transmission electron microscopy; UV-vis, ultraviolet-visible range.

area for interaction with ECs will be greater once the pore size threshold has been met. Anticipating that these GNRs are intended for clinical development in the future, we also considered the possibility of renal and hepatic clearance from the body.[43,44] Therefore, it is important to note that the size of GNRs falls within the range of 10–100 nm to avoid primary clearance.[44] Furthermore, in the body there are many serum proteins that will bind to the particles, increasing the effective particle size.[45]

We confirmed GNR aspect ratio by using the UV-vis feature of our NanoDrop Microvolume Spectrophotometer, which reports an absorption spectrum (Figure 4E). As prior literature indicates that gold nanospheres exhibit just one absorption peak, in this study GNRs absorption spectrum showed two peaks, which can be assigned to the longitudinal and transverse surface plasmon absorption peaks corresponding to the GNR long and short axes, respectively. Knowing that the absorption spectrum varies directly with the aspect ratio of the rods,[46] we identified a peak at around 550 nm (Figure 4E), which corresponds to the short axis, and peak at 740 nm (Figure 4E), which corresponds to the long axis. From the maximum absorption peak wavelength (λ_{max}), we derived a GNR aspect ratio (R) of 3.37 using the approximation $R = (\lambda_{max} - 495.14)/(53.71 \times \varepsilon_m) + 0.79$,[46] where ε_m is the dielectric constant (for water $\varepsilon_m = 1.77$).[47] This aspect ratio

could be confirmed by $R = $ (long axis dimension)/(short axis dimension) $= 27.9$ nm/8.4 nm $= 3.4$, using the TEM measurements. In addition, our absorption spectrum and aspect ratio results agree with the maximum absorption peak wavelengths and aspect ratios reported by Nikoobakht and Feng, who obtained, for example, 700 nm for GNRs of 2.7 aspect ratio, 728 nm for GNRs of 3.4 aspect ratio, and 760 nm for GNRs of 3.9 aspect ratio.[30,48]

PEGylation mitigates GNR toxicity

At present, CTAB-based GNRs[22–36] are well known to be toxic. To address this issue, a few modifications have been incorporated into published CTAB-GNR synthesis protocols. However, the number of cell culture biocompatibility studies that have been conducted to assess toxicity of unmodified and modified CTAB-GNRs is limited. These studies have primarily been performed in non-ECs, including fibroblasts from mouse embryos or human skin, kidney cells from human embryos, hepatocytes from human fetuses, and cells derived from human tumors such as bone marrow neuroblastoma, breast cancer, colorectal cancer, and hepatocellular cancer.[22,32,36] Studies of CTAB-GNR interactions with ECs, relevant to intravascular drug delivery, are rare.[24,26,32,34] Further studies of GNR interactions with ECs are essential, to build knowledge that can translate to

the development of improved GNRs for navigating the EC GCX, a physical barrier to GNR entry into ECs and the blood vessel wall.

So, we performed the necessary toxicity studies here. HUVEC in the absence of GNRs were compared to HUVEC with 500 µg/mL of CTAB-coated GNRs. Despite substantial washing to remove CTAB, after 2 hours of exposure to CTAB-coated GNRs there was a significant decrease in cellular viability, to 54%±10% of the untreated condition (Figure 5A). By 4, 8, 16, and 24 hours, the remaining viable cells reduced to 20%±8.1%, 12%±6.7%, 3%±5.0%, and 2%±3.1%, respectively (Figure 5A). Our toxicity concern has been described in studies previously reported by other research groups, and the mechanism of cellular toxicity of CTAB is currently under investigation.[49,50] In the meantime, CTAB replacement with biocompatible polymers is a widely used solution.[51–53] For our study, we applied this solution by utilizing a heterobifunctional PEG as replacement of CTAB, to eliminate toxicity and promote biocompatibility as in one of our previous studies.[7] PEG replacement of CTAB successfully mitigated toxicity, as indicated by the improved biocompatibility shown in Figure 5A. Successful removal of CTAB and addition of the functional PEG coating was confirmed by reduced toxicity. There was sustained cell viability for up to 24 hours and up to a 1 mg/mL GNR concentration, as seen in Figure 5A, which indicates that our PEG-GNRs are cyto-compatible.

Human EC GCX expression depends on flow and enzyme conditions

Prior to studying how the PEGylated GNRs would interact with the ECs as a function of the GCX, the human ECs were prepared in one of three ways. One way was to treat the ECs with physiological flow, a condition in which we expected human ECs express their most abundant GCX. Another way was to expose the ECs to enzyme in the flow stream, to trigger GCX degradation. A third way was to incubate the ECs in static flow conditions, which was expected would also trigger GCX degradation. The thickness and coverage of HUVEC GCX under these three conditions were quantified by focusing on HS because it is a major component of the GCX. It is important to note, however, that the GCX consists of numerous components that could be explored, limiting the scope of our study.

Figure 6D–F shows fluorescent images of HS on HUVEC in all three conditions. The HS stain shows a healthy HUVEC GCX in flow (Figure 6D) conditions and limited GCX expression in the static (Figure 6E) or flow with enzyme (Figure 6F) conditions. Compared to flow conditions, HS coverage of HUVEC showed a 31.2%±14.8% decrease in static culture and a 75.4%±9.8% decrease in flow conditions with HepIII treatment (Figure 6J). HS thickness dropped from 1.3±0.2 µm for HUVEC in flow conditions to 0.8±0.3 µm for HUVEC in static culture and to 0.6±0.3 µm for HUVEC in flow conditions with HepIII treatment (Figure 6K). This indicated a
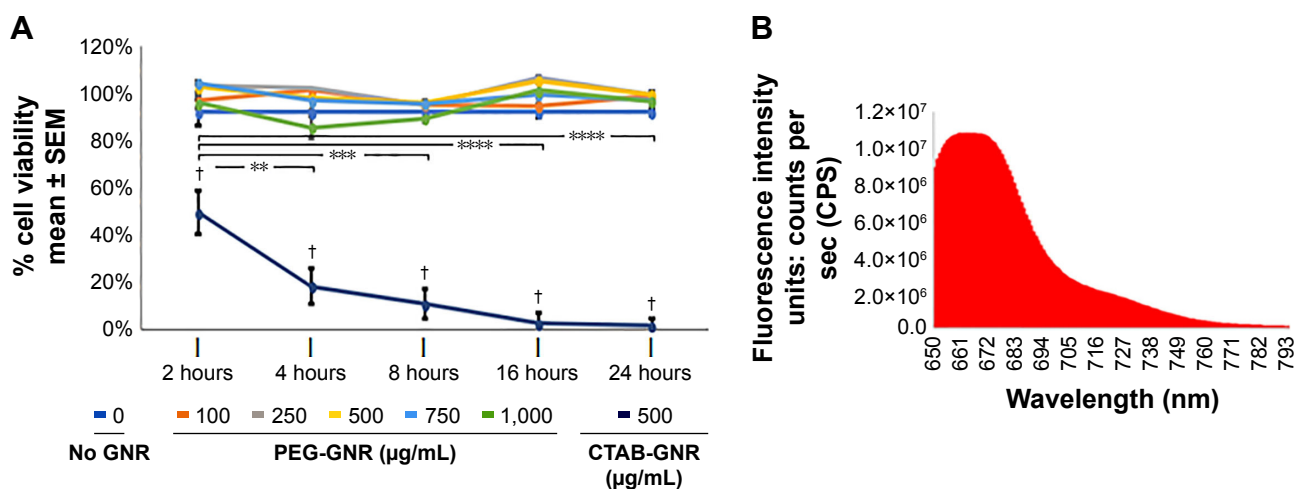

Figure 5 Characterization of PEG-GNR cytotoxicity and fluorescence.
Notes: (**A**) MTS assays were used to examine consistency or changes in metabolic activity of the cells incubated in the absence of GNRs or in the presence of CTAB-GNR or PEG-GNR. MTS indicates that CTAB-GNR, shown in Figure 4A, is toxic for HUVEC. CTAB-GNR treated cells exhibit statistically significantly lower viability, compared to untreated (no GNR) cells, at 2, 4, 8, 16, and 24 hours (significance, denoted by †, was determined by paired t-test). The loss in viability of CTAB-GNR treated cells begins as early as 2 hours in treatment, with viability dropping more significantly by 24 hours (significance, denoted as $**P<0.01$, $***P<0.001$, and $****P<0.0001$, was determined by ANOVA and Tukey's multiple comparison test). On the other hand, PEG-GNR, as depicted in Figure 4B, was found by MTS to show excellent compatibility with HUVEC for up to 24 hours and at up to 1 mg/mL concentration. N=3. (**B**) The AF-647 conjugated PEG-GNR, shown in Figure 4B, has a fluorescence intensity that peaks at 660–670 nm, which coincides with the emission for AF-647 fluorophores.
Abbreviations: CTAB, cetyltrimethylammonium bromide; GNRs, gold nanorods; HUVEC, human umbilical vein endothelial cell; PEG, polyethylene glycol; SEM, standard error of the mean.
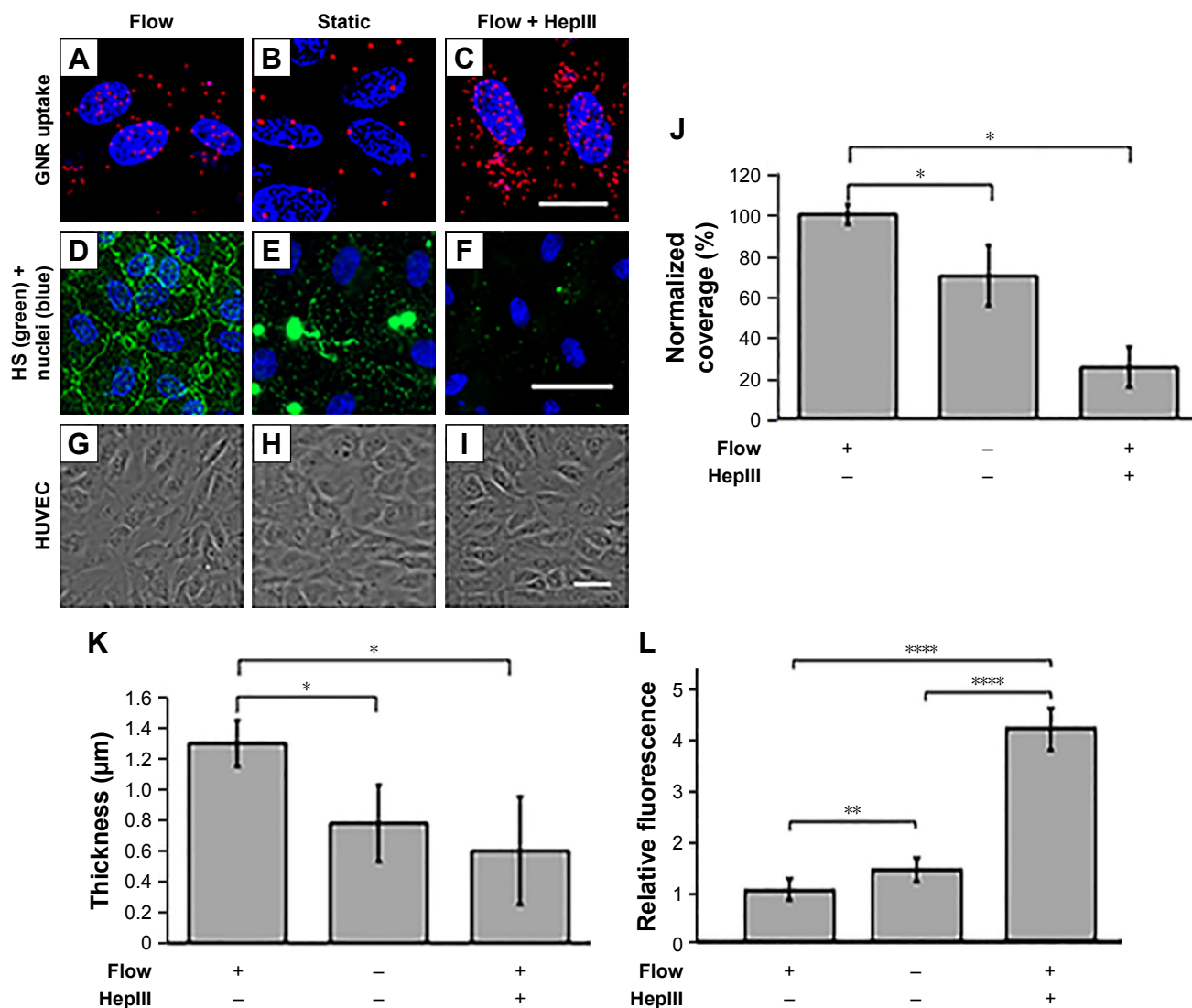
Figure 6 GCX expression and GNR uptake in HUVECs under different enzyme and flow conditions.
Notes: (**A–I**) Images of HUVEC cultures conditioned by 16 hours of 12 dynes/cm^2 shear stress flow, absence of flow, or flow combined with GCX damaged by 1.25×10^{-6} IU/mL HepIII enzyme to degrade HS. (**A–C**) These conditions were followed by 4 hours of incubation with GNRs. The nanoparticles are shown in red and HUVEC nuclei are shown in blue. Scale bar =20 μm. (**D–F**) Confocal images of HUVEC cultures stained for the HS component of GCX, for all three conditions. Scale bar =50 μm. (**G–I**) Phase contrast images show healthy HUVEC morphology, indicating HUVEC compatibility with GNR treatments. Scale bar =50 μm. (**J–L**) GCX measurements of GCX coverage (**J**), GCX thickness (**K**), and corresponding GNR uptake (**L**). Data shown are mean ± SEM. *$P<0.05$, **$P<0.01$, ****$P<0.0001$, and $3<N<5$.
Abbreviations: GCX, glycocalyx; GNRs, gold nanorods; HUVEC, human umbilical vein endothelial cell.

significant difference in GCX composition when the three conditions were compared to each other, suggesting that there would be differences in GNR permeability.

HUVEC permeability to GNRs is correlated to GCX conditions

Conjugation of AF-647 to the PEG on our GNRs was confirmed by fluorescence measurements which showed an emission peak at 660-670 nm matching AF-647 emission wavelength (Figure 5B). This AF-647 conjugation facilitates confocal fluorescence visualization of GNR infiltration into cultured HUVEC that are incubated with 500 mg/mL GNRs for 4 hours. The 4-hour co-incubation of HUVEC and GNRs

occurs after 16 hours of no flow, or flow at 12 dynes/cm^2 shear stress with or without 1.25×10^{-6} IU/mL HepIII.

As an outcome of HUVEC and GNR co-incubation, GNRs are taken up by the ECs in all conditions (Figure 6A–C). The lowest level of GNR permeability was observed in flow conditions (Figure 6A), which corresponds to healthy GCX (Figure 6D). The levels of permeability increase in static or HepIII conditions (Figure 6B, C) with decrease in stabilization of the GCX (Figure 6E, F). GNR uptake by ECs causes no visible morphological changes to the cells (Figure 6G–I). Quantification of these observations revealed that, compared to flow-conditioned HUVEC, cells in static conditions where GCX exhibited approximately 31% and ~40% degradation in

coverage (Figure 6J) and thickness (Figure 6K), were found to be 1.4-fold more permeable to the GNRs (Figure 6L). Cells in conditions of flow with 1.25×10^{-6} IU/mL HepIII, where GCX coverage dropped by 75% (Figure 6J) and GCX thickness dropped by ~45% (Figure 6K), were found to be the most permeable to GNRs, showing a 4.1-fold increase compared to conditions of only flow (Figure 6L).

These permeability results confirm that GNR uptake by ECs is inversely correlated to the state of the GCX on the ECs (Figure 6J–L). However, onset of GCX deficiency conditions (with the absence of flow) was not enough to substantially increase EC permeability to these GNRs (Figure 6L). This can be seen as an unexpected limitation of our GNRs, because the atherosclerosis-prone blood vessel regions that we want to target coincide with disruptions in streamlined flow which include stagnation.[54] The high surface area of the GNR long axis may be blocking passive GNR uptake by static-conditioned ECs, because while the GCX is degraded in static conditions, the porosity is still smaller than the long axes of the GNRs.[55] In addition, our synthesized GNRs omit targeting moieties which would facilitate particle delivery into the ECs.[56] We found that advanced GCX deficiency conditions (with flow combined with HepIII treatment) were required for marked elevation in EC permeability to GNRs (Figure 6L).

HUVEC permeability to GNRs is more efficient than permeability to gold nanospheres

We previously showed that 10 nm PEG-coated gold spherical nanoparticles have significantly high rates of infiltration into vascular ECs with compromised GCX.[7] Therefore, the present GNR permeability results appear to be similar to our previously reported finding.[7] However, in preliminary-level studies we found a statistical difference between GCX-mediated human endothelial uptake of GNRs and GCX-mediated EC uptake of gold nanospheres. We performed this preliminary-level experiment using cells that were deficient in GCX due to static culture conditions. The cells were co-incubated with 500 µg/mL of nanoparticles for 2, 4, 8, and 16 hours (Figure 7). We found that the GNRs, in comparison with the previously investigated gold nanospheres,[7] exhibited a faster uptake into GCX-deficient human ECs. After 2 hours of incubating nanoparticles of both morphologies with the ECs, GNR infiltration in ECs was 2.4-fold higher than gold nanospheres infiltration (Figure 7A, E, I, M, and Q). At a 4-hour time point, a lesser difference between

endothelial permeability to nanoparticles of the two morphologies was observed, with 1.4-fold higher permeability of rods versus spheres (Figure 7B, F, N, and Q). At 8 and 16 hours, we observed that EC permeability to GNRs was higher than permeability to gold nanospheres by 21.1% and 11.8%, respectively (Figure 7C, D, G, H, K, L, O, Q). These results strongly demonstrate the advantage of GNRs over gold nanospheres. More interestingly, it was at the earlier time points when GNRs strongly demonstrated their advantage over gold nanospheres. At a 4-hour time point, a larger difference between endothelial permeability to nanoparticles of the two morphologies was observed, with 1.4-fold higher permeability of rods vs spheres (Figure 7B, F, J, N and Q). After 2 hours of incubating nanoparticles of both morphologies with the ECs, GNR infiltration in ECs was 2.4-fold higher than gold nanospheres infiltration (Figure 7A, E, I, M and Q).

Similar comparative studies were performed by other groups,[57,58] although the role of the GCX was not examined in these other studies. Agarwal and team observed that nanorods were taken up with higher efficiency than nanospheres.[57] Kolhar and Mitragotri found no statistical difference in endothelial permeability to nanoneedles vs nanospheres, but reported higher efficiency of siRNA delivery from the nanoneedles compared to the nanospheres.[58] As we stated earlier, the results reported here by us and in the reports by Agarwal et al[57] and by Kolhar and Mitragotri[58] can be explained by the fact that rod (or needle) shaped nanoparticles have larger surface areas for interactions with cell membranes.[21,59,60] In other words, while gold nanosphere contact with the EC membrane is minimal, there is a wider extent of contact between the GNRs and EC membrane.[57] Based on this understanding, we speculate that in the absence of the GCX barrier, the adhesion forces that engage GNRs and the EC membrane will be higher than the forces that engage gold nanospheres with the EC membrane.[57] Agarwal's team proposed an additional explanation: the GNRs are slightly larger than the gold nanospheres, giving the GNRs more weight and, as a result, encouraging them to settle more of the EC membrane.[57] High adhesion forces combined with high rate of settling on the cell membrane fully explains why GNR permeability into ECs can be greater than gold nanosphere permeability.

One might assume that the surface charges of the nanoparticles could serve as an additional explanation for why GNR particle permeability is more efficient than its gold nanosphere counterpart. However, in our study, both
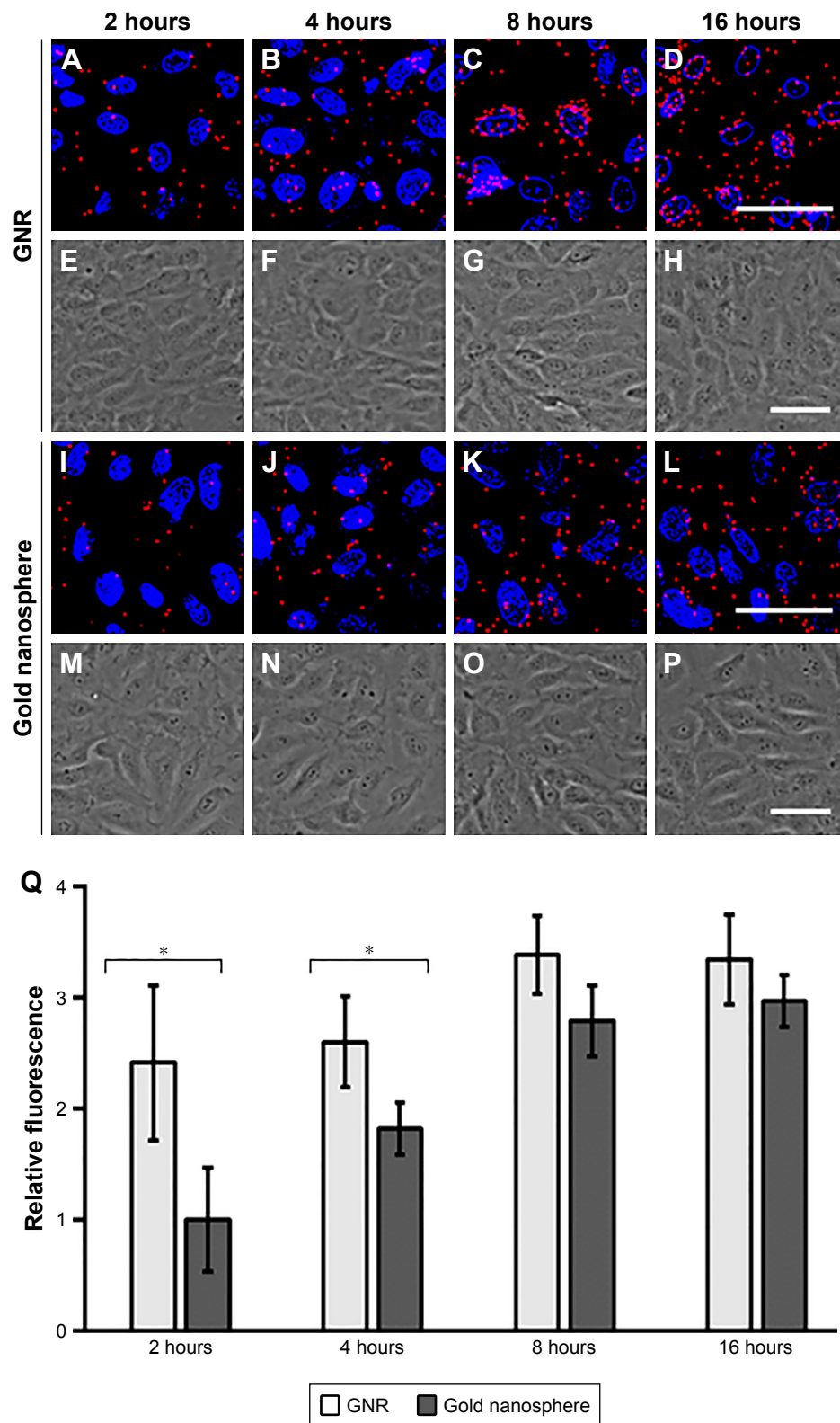
Figure 7 Confocal images of static HUVEC cultures incubated with 500 μg/mL GNR (**A–D**) or gold nanospheres (**I–L**) for 2, 4, 8, and 16 hours are shown; scale bar =50 μm. The nanoparticles are shown in red and HUVEC nuclei are shown in blue. Phase contrast images of healthy HUVEC morphology, indicating HUVEC compatibility with GNR (**E–H**) or gold nanosphere (**M–P**) treatments are also shown; scale bar =20 μm. The bar plot (**Q**) shows comparative uptake of the nanoparticles over time in static cultured HUVEC. GNRs infiltrate HUVEC faster than gold nanospheres. Both particle shapes plateau at 8–16 hours, but GNR show significant uptake over gold nanosphere at 2 and 4 hours. The data are normalized to fluorescence of gold nanospheres at 2 hours, and presented as mean ± SEM. Statistical significance is indicated by *$P < 0.05$. N=5.
Abbreviations: GNRs, gold nanorods; HUVEC, human umbilical vein endothelial cell; SEM, standard error of the mean.

particles were intentionally synthesized with the same PEG coating, which is slightly negative in charge, as we previously reported.[7] Given that the GCX is also negatively charged, repulsion forces will block interaction between the intact GCX and negatively charges nanoparticles[61,62] of either rod or sphere morphologies. GNRs and gold nanospheres will both show uptake as the GCX begins to degrade, which will lead to the EC membrane becoming less negatively charged, making it possible for us to evaluate nanoparticle permeability differences independent of surface charge differences and purely due to the physical characteristic differences between the nanoparticles.
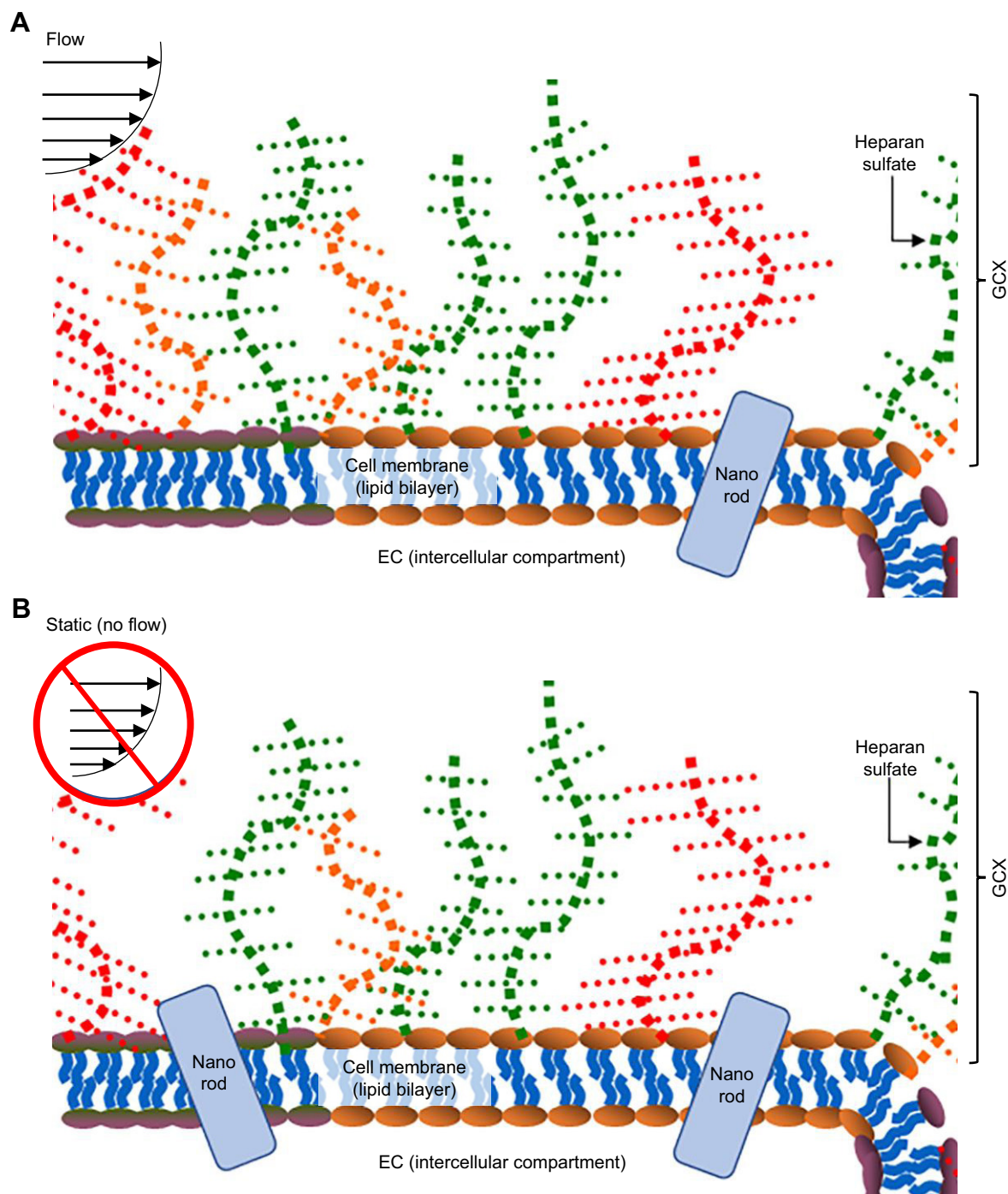
Figure 8 (*Continued*)
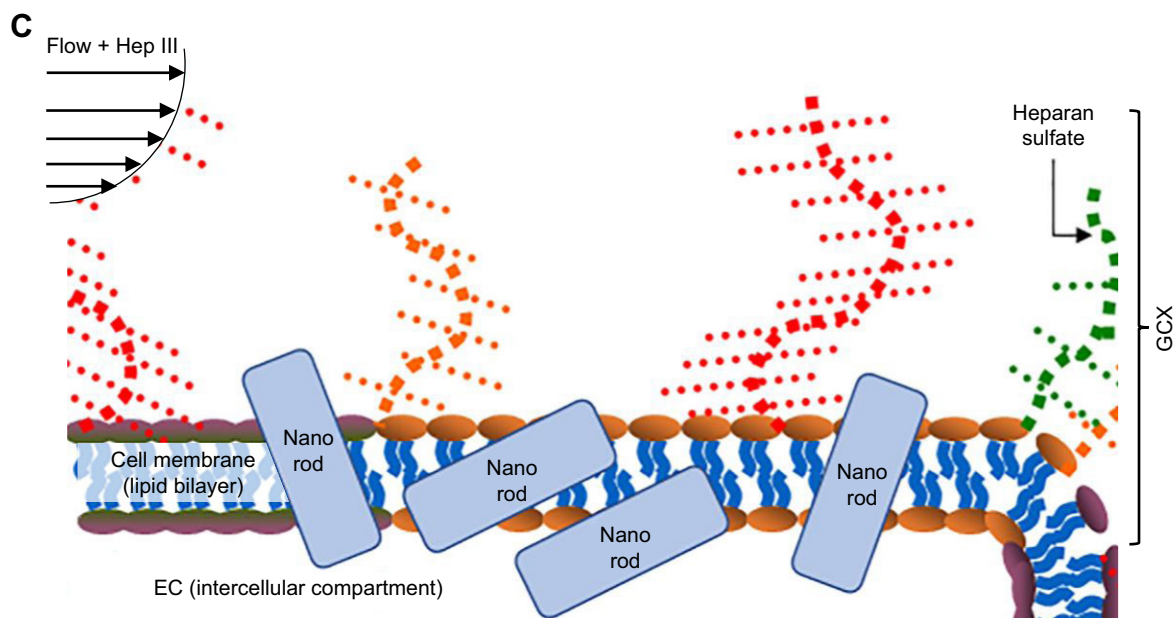
Figure 8 Conceptual model of how HUVECs interact with GNRs.
Notes: (**A**) Flow-conditioned HUVECs exhibit robust GCX that blocks most of the cellular interaction with GNRs. (**B**) If HUVECs are taken out of the flow environment, the GCX is destabilized, for a limited increased in GNR uptake by HUVECs. (**C**) Adding to the flow stream GCX degradation enzyme (eg, HepIII to degrade HS) leads to more destabilization of the GCX and opens more avenues for GNRs to penetrate the cells, leading to greater uptake. (The GNRs and ECs are not drawn to scale.)
Abbreviations: EC, endothelial cell; GNRs, gold nanorods; GCX, glycocalyx; HUVEC, human umbilical vein endothelial cell.

Conclusion

This work aimed to develop a nanoscale vehicle that would pass through the nanoporous endothelial GCX as it degrades and as its porosity increases. Towards this aim, we describe a new method to develop GNRs that, compared to previously published versions,[22–36] are ultrasmall and better suited for GCX penetration. Further unlike many developers of nanoparticle drug delivery vehicles who have not carefully considered the GCX, we investigated GCX-mediated endothelial permeability to these GNRs. Our results confirm that ultrasmall GNR permeability is inversely correlated to the state of the GCX as depicted in the conceptual model (Figure 8A–C). When considering that our long-term goal is to target and treat atherosclerosis-prone blood vessels, which have degraded GCX, we expect that these GNRs will be advantageous for increased delivery of any drugs being carried to diseased blood vessel regions.

Although this work lays the foundation for future translational to the clinic, there are limitations. One limitation is that our focus on the GCX is limited to only HS, which is just one of numerous GCX components. A second limitation is that our nanoparticles are only functionalized to block toxicity and for fluorescent visualization, not including functionalization for active targeting and drug delivery which are also important. A third limitation is that the scope of this study is limited to in vitro studies and the results are not verified in vivo, leaving the translational potential of this work unknown. In future studies, it will be critical for us to study this passive GCX-mediated GNR infiltration into ECs in vivo, to identify the threshold of GCX degradation at which GNRs can penetrate ECs, and to explore the role of multiple GCX components. Furthermore, it will be important to functionalize our GNRs to deliver anti-atherosclerosis drugs in a timely, targeted, and effective fashion.

Acknowledgments

Author contributions

MJC, RK, and EEE designed the experiments. MJC, PP, and NNB performed the experiments and analyzed the data. MJC, NNB, and EEE interpreted the results of the experiments. NNB, MJC, PP, and EEE drafted the figures and manuscript. NNB, TJW, SS, and EEE edited, revised, and approved the final manuscript. TJW, SS, and EEE supervised the project. All authors contributed to data analysis, drafting and revising the article, gave final approval of the version to be published, and agree to be accountable for all aspects of the work.

Disclosure

The authors report no conflicts of interest in this work.

References

1. Laroia ST, Ganti AK, Laroia AT, Tendulkar KK. Endothelium and the lipid metabolism: the current understanding. *Int J Cardiol*. 2003;88(1):1–9.
2. Benjamin EJ, Blaha MJ, Chiuve SE, et al; American Heart Association Statistics Committee and Stroke Statistics Subcommittee. Heart disease and stroke statistics-2017 update: a report from the American Heart Association. *Circulation*. 2017;135(10):e146–e603.
3. Cancel LM, Ebong EE, Mensah S, Hirschberg C, Tarbell JM. Endothelial glycocalyx, apoptosis and inflammation in an atherosclerotic mouse model. *Atherosclerosis*. 2016;252:136–146.
4. Kolářová H, Ambrůzová B, Svihálková Šindlerová L, Klinke A, Kubala L. Modulation of endothelial glycocalyx structure under inflammatory conditions. *Mediators Inflamm*. 2014;2014:694312.
5. Lewis J, Taylor RG, Jones N, St Clair R, Cornhill J. Endothelial surface characteristics in pigeon coronary artery atherosclerosis I. Cellular alterations during the initial stages of dietary cholesterol challenge. *Lab Invest*. 1982;46(2):123–138.
6. van den Berg BM, Spaan JA, Rolf TM, Vink H. Atherogenic region and diet diminish glycocalyx dimension and increase intima-to-media ratios at murine carotid artery bifurcation. *Am J Physiol Heart Circ Physiol*. 2006;290(2):H915–H920.
7. Cheng MJ, Kumar R, Sridhar S, Webster TJ, Ebong EE. Endothelial glycocalyx conditions influence nanoparticle uptake for passive targeting. *Int J Nanomed*. 2016;11:3305–3315.
8. Tarbell JM, Ebong EE. The endothelial glycocalyx: a mechano-sensor and -transducer. *Sci Signal*. 2008;1(40):pt8.
9. Reitsma S, Slaaf DW, Vink H, van Zandvoort MA, oude Egbrink MG. The endothelial glycocalyx: composition, functions, and visualization. *Pflugers Arch*. 2007;454(3):345–359.
10. Cavallo C, Di Pascasio F, Latini A, Bonomo M, Dini D. Nanostructured semiconductor materials for dye-sensitized solar cells. *J Nanomater*. 2017;2017(3):1–31.
11. Hanif I, Camara O, Tunes MA, et al. Ion-beam-induced bending of semiconductor nanowires. *Nanotechnology*. 2018;29(33):335701.
12. Krishnan N, Boyd S, Somani A, Raoux S, Clark D, Dornfeld D. A hybrid life cycle inventory of nano-scale semiconductor manufacturing. *Environ Sci Technol*. 2008;42(8):3069–3075.
13. Weir A, Westerhoff P, Fabricius L, Hristovski K, von Goetz N. Titanium dioxide nanoparticles in food and personal care products. *Environ Sci Technol*. 2012;46(4):2242–2250.
14. Mirza AZ, Siddiqui FA. Nanomedicine and drug delivery: a mini review. *Int Nano Lett*. 2014;4(1):94.
15. Cho EJ, Holback H, Liu KC, Abouelmagd SA, Park J, Yeo Y. Nanoparticle characterization: state of the art, challenges, and emerging technologies. *Mol Pharm*. 2013;10(6):2093–2110.
16. De Jong WH, Borm PJ. Drug delivery and nanoparticles:applications and hazards. *Int J Nanomedicine*. 2008;3(2):133–149.
17. Davis ME, Chen Z, Shin DM. Nanoparticle therapeutics: an emerging treatment modality for cancer. *Nat Rev Drug Discov*. 2008;7(9):771–782.
18. Chinen AB, Guan CM, Ferrer JR, Barnaby SN, Merkel TJ, Mirkin CA. Nanoparticle probes for the detection of cancer biomarkers, cells, and tissues by fluorescence. *Chem Rev*. 2015;115(19):10530–10574.
19. Moghimi SM, Hunter AC, Murray JC. Nanomedicine: current status and future prospects. *FASEB J*. 2005;19(3):311–330.
20. Wagner V, Dullaart A, Bock AK, Zweck A. The emerging nanomedicine landscape. *Nat Biotechnol*. 2006;24(10):1211–1217.
21. Liu Y, Tan J, Thomas A, Ou-Yang D, Muzykantov VR. The shape of things to come: importance of design in nanotechnology for drug delivery. *Ther Deliv*. 2012;3(2):181–194.
22. Adura C, Guerrero S, Salas E, et al. Stable conjugates of peptides with gold nanorods for biomedical applications with reduced effects on cell viability. *ACS Appl Mater Interfaces*. 2013;5(10):4076–4085.
23. Ahmed W, Bhatti AS, van Ruitenbeek JM. Efficient seed-mediated method for the large-scale synthesis of Au nanorods. *J Nanopart Res*. 2017;19(3):115.
24. Beji Z, Hanini A, Smiri LS, et al. Magnetic properties of Zn-substituted MnFe$_2$O$_4$ nanoparticles synthesized in polyol as potential heating agents for hyperthermia. Evaluation of their toxicity on endothelial cells. *Chem Mater*. 2010;22(19):5420–5429.
25. da Silva JA, Meneghetti MR. New aspects of the gold nanorod formation mechanism via seed-mediated methods revealed by molecular dynamics simulations. *Langmuir*. 2018;34(1):366–375.
26. Fish MB, Thompson AJ, Fromen CA, Eniola-Adefeso O. Emergence and utility of nonspherical particles in biomedicine. *Ind Eng Chem Res*. 2015;54(16):4043–4059.
27. Jessl S, Tebbe M, Guerrini L, Fery A, Alvarez-Puebla RA, Pazos-Perez N. Silver-assisted synthesis of gold nanorods: the relation between silver additive and iodide impurities. *Small*. 2018;14(20):1703879.
28. Kaur P, Chudasama B. Effect of colloidal medium on the shelf-life and stability of gold nanorods prepared by seed-mediated synthesis. *J Nanosci Nanotechnol*. 2018;18(3):1665–1674.
29. Khlebtsov BN, Khanadeev VA, Khlebtsov NG. Extinction and extra-high depolarized light scattering spectra of gold nanorods with improved purity and dimension tunability: direct and inverse problems. *Phys Chem Chem Phys*. 2014;16(12):5710–5722.
30. Nikoobakht B, El-Sayed MA. Preparation and growth mechanism of gold nanorods (NRs) using seed-mediated growth method. *Chem Mater*. 2003;15(10):1957–1962.
31. Park K, Hsiao MS, Yi YJ. Highly Concentrated Seed-Mediated Synthesis of Monodispersed Gold Nanorods. *ACS Applied Materials & Interfaces*. 2017;9(31):26363–26371.
32. Santhosh PB, Thomas N, Sudhakar S, Chadha A, Mani E. Phospholipid stabilized gold nanorods: towards improved colloidal stability and biocompatibility. *Phys Chem Chem Phys*. 2017;19(28):18494–18504.
33. Sharma S, Bora PJ, Gogoi P, Boruah R, Mohan KJ, Dolui SK. Plasmonic bulk heterojunction photovoltaic devices based on poly (9-vinylcarbazole)/gold nanocomposites: effect of aspect ratio of gold nanorod. *J Mater Sci*. 2015;26(7):5465–5474.
34. Yang H, Chen Z, Zhang L, et al. Mechanism for the cellular uptake of targeted gold nanorods of defined aspect ratios. *Small*. 2016;12(37):5178–5189.
35. Ye X, Gao Y, Chen J, Reifsnyder DC, Zheng C, Murray CB. Seeded growth of monodisperse gold nanorods using bromide-free surfactant mixtures. *Nano Lett*. 2013;13(5):2163–2171.
36. Yu C, Varghese L, Irudayaraj J. Surface modification of cetyltrimethylammonium bromide-capped gold nanorods to make molecular probes. *Langmuir*. 2007;23(17):9114–9119.
37. Khan Z, Singh T, Hussain JI, Hashmi AA. Au(III)-CTAB reduction by ascorbic acid: preparation and characterization of gold nanoparticles. *Colloids Surf B Biointerfaces*. 2013;104:11–17.
38. Ahmed W, Bhatti AS, van Ruitenbeek JM. Efficient seed-mediated method for the large-scale synthesis of Au nanorods. *J Nanopart Res*. 2017;19(3):115.

39. Sharma V, Park K, Srinivasarao M. Shape separation of gold nanorods using centrifugation. *Proc Natl Acad Sci U S A*. 2009;106(13): 4981–4985.

40. Xiong W, Sikdar D, Walsh M, et al. Single-crystal caged gold nanorods with tunable broadband plasmon resonances. *Chem Commun (Camb)*. 2013; 49(83):9630–9632.

41. Smith DK, Korgel BA. The importance of the CTAB surfactant on the colloidal seed-mediated synthesis of gold nanorods. *Langmuir*. 2008; 24(3):644–649.

42. Park K, Drummy LF, Wadams RC, et al. Growth mechanism of gold nanorods. *Chem Mater*. 2013;25(4):555–563.

43. Longmire M, Choyke PL, Kobayashi H. Clearance properties of nano-sized particles and molecules as imaging agents: considerations and caveats. *Nanomedicine (Lond)*. 2008;3(5):703–717.

44. Alexis F, Pridgen E, Molnar LK, Farokhzad OC. Factors affecting the clearance and biodistribution of polymeric nanoparticles. *Mol Pharm*. 2008;5(4):505–515.

45. Wang P, Wang X, Wang L, Hou X, Liu W, Chen C. Interaction of gold nanoparticles with proteins and cells. *Sci Technol Adv Mater*. 2015; 16(3):034610.

46. Link S, El-Sayed MA. Simulation of the optical absorption spectra of gold nanorods as a function of their aspect ratio and the effect of the medium dielectric constant. *J Phys Chem B*. 2005;109(20):10531–10532.

47. Hobbs ME, Jhon MS, Eyring H. The dielectric constant of liquid water and various forms of ice according to significant structure theory. *Proc Natl Acad Sci U S A*. 1966;56(1):31–38.

48. Feng L, Xuan Z, Ma J, et al. Preparation of gold nanorods with different aspect ratio and the optical response to solution refractive index. *J Exp Nanosci*. 2015;10(4):258–267.

49. Alkilany AM, Nagaria PK, Hexel CR, Shaw TJ, Murphy CJ, Wyatt MD. Cellular uptake and cytotoxicity of gold nanorods: molecular origin of cytotoxicity and surface effects. *Small*. 2009;5(6):701–708.

50. Da S, Lc F, Kim U, Romsted L, Sim S; Rutgers Department of Biomedical Engineering, Rutgers, The State University of New Jersey, New Brunswick. *The Source of Toxicity in CTAB and CTAB-Stabilized Gold Nanorods [Master of Science]*; 2013.

51. Hamon C, Bizien T, Artzner F, Even-Hernandez P, Marchi V. Replacement of CTAB with peptidic ligands at the surface of gold nanorods and their self-assembling properties. *J Colloid Interface Sci*. 2014;424:90–97.

52. Zhang Z, Lin M. Fast loading of PEG–SH on CTAB-protected gold nanorods. *RSC Adv*. 2014;4(34):17760–17767.

53. Tebbe M, Kuttner C, Männel M, Fery A, Chanana M, Stable C. Colloidally stable and surfactant-free protein-coated gold nanorods in biological media. *ACS Appl Mater Interfaces*. 2015;7(10):5984–5991.

54. Sui B, Gao P, Lin Y, Gao B, Liu L, An J. Blood flow pattern and wall shear stress in the internal carotid arteries of healthy subjects. *Acta Radiol*. 2008;49(7):806–814.

55. Li Y, Kröger M, Liu WK. Shape effect in cellular uptake of PEGylated nanoparticles: comparison between sphere, rod, cube and disk. *Nanoscale*. 2015;7(40):16631–16646.

56. Marangoni VS, Cancino-Bernardi J, Zucolotto V, Synthesis ZV. Synthesis, physico-chemical properties, and biomedical applications of gold nanorods – a review. *J Biomed Nanotechnol*. 2016;12(6):1136–1158.

57. Agarwal R, Singh V, Jurney P, Shi L, Sreenivasan SV, Roy K. Mammalian cells preferentially internalize hydrogel nanodiscs over nanorods and use shape-specific uptake mechanisms. *Proc Natl Acad Sci U S A*. 2013; 110(43):17247–17252.

58. Kolhar P, Doshi N, Mitragotri S. Polymer Nanoneedle-Mediated Intracellular Drug Delivery. *Small*. 2011;7(14):2094–2100.

59. Barua S, Yoo JW, Kolhar P, Wakankar A, Gokarn YR, Mitragotri S. Particle shape enhances specificity of antibody-displaying nanoparticles. *Proc Natl Acad Sci U S A*. 2013;110(9):3270–3275.

60. Muro S, Garnacho C, Champion JA, et al. Control of endothelial targeting and intracellular delivery of therapeutic enzymes by modulating the size and shape of ICAM-1-targeted carriers. *Mol Ther*. 2008;16(8): 1450–1458.

61. Harush-Frenkel O, Rozentur E, Benita S, Altschuler Y. Surface charge of nanoparticles determines their endocytic and transcytotic pathway in polarized MDCK cells. *Biomacromolecules*. 2008;9(2):435–443.

62. Huang RB, Mocherla S, Heslinga MJ, Charoenphol P, Eniola-Adefeso O. Dynamic and cellular interactions of nanoparticles in vascular-targeted drug delivery (review). *Mol Membr Biol*. 2010;27(4–6):190–205.

63. He J, Zheng W, Ligmajer F, et al. Plasmonic enhancement and polarization dependence of nonlinear upconversion emissions from single gold nanorod@SiO2@CaF2:Yb3+,Er3+ hybrid core–shell–satellite nanostructures. *Light: Science & Applications*. 2017;6(5).